Chemical Engineering Journal 371 (2019) 301–305

Contents lists available at ScienceDirect

Chemical Engineering Journal

journal homepage: www.elsevier.com/locate/cej

Short communication

Designing bioresponsive metal azolate framework-based nanosystem for efficient cancer therapy

Chengcheng Sang[1], Li Ma[1], Dong Luo, Hongxing Liu, Dan Li*, Tianfeng Chen*

College of Chemistry and Materials Science, Jinan University, Guangzhou 510632, China

HIGHLIGHTS

- A novel pH-responsive Metal Azolate Framework-based nanosystem is designed and synthesized.
- The designed nanosystem can deliver therapeutic selenadiazole derivative to cancer cells with high-efficiency.
- The designed system can precisely and significantly inhibited tumor growth.

ARTICLE INFO

Keywords:
Metal azolate framework
Nanosystem
Bioresponsive
Precise cancer therapy

ABSTRACT

Chemotherapy is one of the major cancer therapeutic approaches, however, it is limited by non-specificity, poor solubility, resistance. We reported here the use of bioresponsive nano metal azolate framework-4 (MAF-4) as vehicle materials and cRGD (cyclic arginine-glycine-aspartic) as target peptide to precisely deliver PSeD (selenadiazole derivative) to breast cancer cells. This intelligent nanosystem was stable at relatively basic pH (~7.4, body fluid), while it slowly decomposed at slightly acidic pH (~5.3, lysosomes) to release drug for precise treatment of breast cancer. The nanosystem specifically accumulated in tumors *in vivo*, and thus demonstrated high antitumor efficacy and non-toxic to normal tissues. Generally, this study indulged an innovative strategy for efficient cancer therapy using intelligent nanocarrier materials.

Breast Cancer is the most common gynecological malignancies, representing the most serious threat of death among women worldwide [1]. Chemotherapy is one of the major standard therapeutic approaches, however, it is obviously limited by non-specificity, poor solubility, resistance and unknown side effects [2]. New strategies to overcome these drawbacks are urgently needed. Integrin $\alpha_v\beta_3$, a receptor for RGD (arginine-glycine-aspartic) or cyclic RGD (cRGD) peptides, is overexpressed on activated endothelial cells and tumor cells [3], which provided an efficient avenue for designing targeting drugs to combat breast cancer. In the meantime, selenadiazole derivatives (SeDs) have been identified as a new potential drug to treat breast cancer by regulation of apoptotic signaling pathways [4–6]. PSeD (Fig. S1), the best SeDs reported until now with excellent anticancer activity and good inhibitory effect was selected in this work. However, the poor solubility and insufficient selectivity of PSeD limit its clinical application. In order to solve these problems, developing novel biocompatible intelligent hybrid vehicle materials to selectively delivery PSeD to tumor cell is required. In the meanwhile, metal-organic frameworks are novel materials with great potential in biomedicine delivery due to their high modifiability to form hybrid materials [7–13]. Herein we report the first use of bioresponsive and biocompatible nanoscale metal-azolate framework-4 (MAF-4) conjugated with cRGD and copolymer as hybrid vehicle system (PSeD@MAF-4(R)) for the effective delivery of PSeD to breast cancer cells (Fig. 1).

MAF-4 is synthesized from acid-base neutralization reaction between 2-methylimidazole and $Zn(NO_3)_2$, presenting a 3D intersecting pore system [14]. MAF-4 shows variable applications due to the high surface areas and large uniform pore sizes. More importantly, the nature of MAF-4 determined it is pH-sensitive since MAF-4 is the product obtained from acid-base neutralization reaction [15–17]. On the other hand, biological system is also well known to be highly pH sensitive and different cell organelles have different acidity. These make MAF-4 system can be potentially used as a smart biorespective vehicle materials to deliver drugs *in vivo* once scaled down to nanoscale (Fig. 1) [9,18–20]. MAF-4 nanosystem not only maintains the structure and physicochemical properties as bulk MAF-4 but also exhibits nano size

* Corresponding authors.
E-mail addresses: danli@jnu.edu.cn (D. Li), tchentf@jnu.edu.cn (T. Chen).
[1] These authors contributed equally to this work.

https://doi.org/10.1016/j.cej.2019.04.016
Received 7 February 2019; Received in revised form 27 March 2019; Accepted 3 April 2019
Available online 04 April 2019
1385-8947/

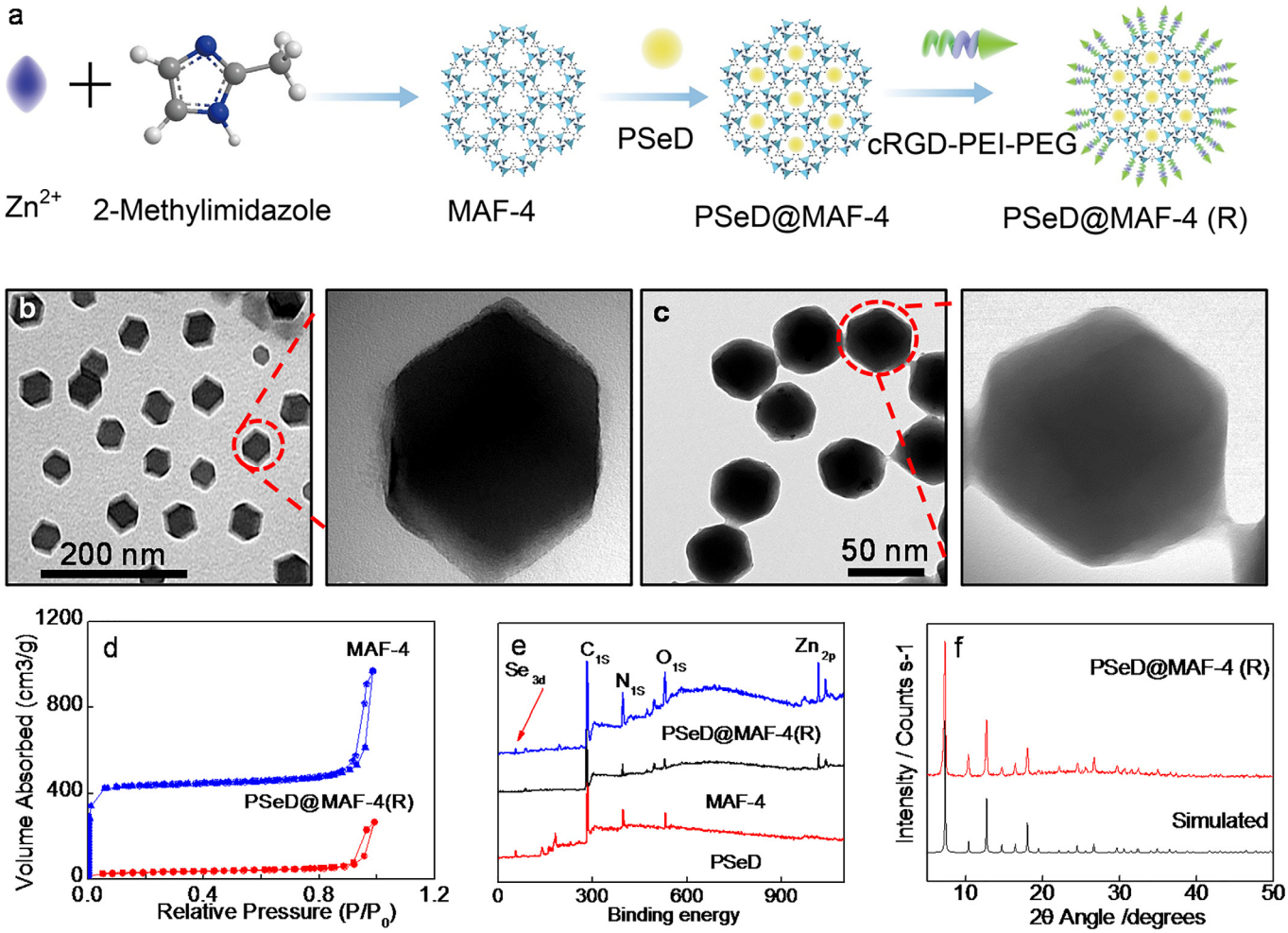

Fig. 1. a) Design and preparation of PSeD@MAF-4(R). TEM image of MAF-4 (b) and PSeD@MAF-4(R) (c). d) BET surface area. e) XPS spectra. f) PXRD characterization of simulated MAF-4 and PSeD@MAF-4(R).

effects suitable for drug delivery [21–26]. In our system, the large uniform pore of MAF-4 provides a platform to load PseD (loading rate 16.1 ± 0.9%), while the high surface area offers more surface metal ion to facilitate functionalization with biocompatible polymers [27,28].

In this study, we scaled down MAF-4 to 40 nm as nanocarrier material [29], and then loaded PseD to MAF-4 through mesoporous adsorption to form PseD@MAF-4 (Fig. 1a). In order to link cRGD targeting peptide to PseD@MAF-4, we employed polyethylenimine-polyethylene glycol (PEI-PEG) as copolymers to form a two cross-linked di-block linker [30]. The nanoparticle characterization was done very carefully after current recommendation [7,8] to confirm their monodispersity and colloidal stability. From TEM images (Fig. 1b) and N_2 absorption-desorption isotherm (Figs. 1d and S2a) results, we confirmed that the synthesized MAF-4 is highly dispersed hexagonal plate-like nanoparticles with diameter at ~40 nm and maintained porous property (with BET specific surface area 1345 cm^3/g). After PSeD loading and cRGD decoration, PseD@MAF-4(R) nanosystem was also crystal (Fig. 1f) and uniformly dispersed with a thin film on the edge (Fig. 1c), while the BET surface area was significantly decreased to 105 cm^3/g (Fig. 1d). The loading rate of PSeD was found at 16.1 ± 0.9%, and further confirmed by XPS (Fig. 1e) and UV–Vis spectra analysis (Fig. S2b). The successful conjugation of cRGD was also evidenced by BCA protein assay (Fig. S2c) and infrared spectrum (Fig. S2d).

MAF-4 is stable at relatively basic pH, while it will slowly decomposes at acidic pH. This property was confirmed in MCF-7 human breast cancer cells. Firstly, we studied the localization of the MAF-4 using fluorescence microscopy. As shown in Fig. 2a and 2b, PSeD@MAF-4(R) was absorbed into the cells by endocytosis after 1 h incubation, and localized in lysosomes (pH 5.3) at the end time. PSeD released from PSeD@MAF-4(R) after 2 h, and the green fluorescence of PSeD slowly increased with time, finally filled the whole cytoplasm at 4 h. The mechanism of PSeD@MAF-4(R) endocytosis was further confirmed by using various endocytosis inhibitors (Fig. S3). The pH bioresponse was further examined by powder X-ray diffraction (PXRD) in a varity of physiological conditions (Fig. 2c). The results shown that, MAF-4 nanosystem was stable under the tested physiological conditions after one week, while decomposed at pH 5.3. This may be due to the ligand protonation in acidic pH. Once the ligand protonated, the coordination ability decreased. The TEM images shown that, after treatment with pH = 5.3 buffer for 1 h, the particle size of PSeD@MAF-4(R) increased siginificantly, while maintained the same shape and size at pH 7.4 (Fig. 2d). The dynamic light scattering (DLS) results also confirmed this phenomenon (Fig. S4).

Drug release experiments was also carried out at pH 7.4 and 5.3. As shown in Fig. 2e, PSeD was released from PSeD@MAF-4(R) from 16.5% (4 h) to 29.1% (24 h) in pH 7.4 buffer, while in pH 5.3 buffer, PSeD release rate reached 47.8% (24 h). The stability of PseD@MAF-4(R) system under physiological conditions was studied by monitoring its particle size in PBS using DLS (Fig. S5a). No obvious particle size change was observed after one week, which indicated that this system was very stable in physiological media and suitable for *in intro* and *in vivo* experiments. Interestingly, the Zeta potential of PseD@MAF-4(R) was much higher (+35 mV) than the naked MAF-4 (+20 mV), possibly due to the cationic polymer PEI wrapping (Fig. S5b), thus enhanced the

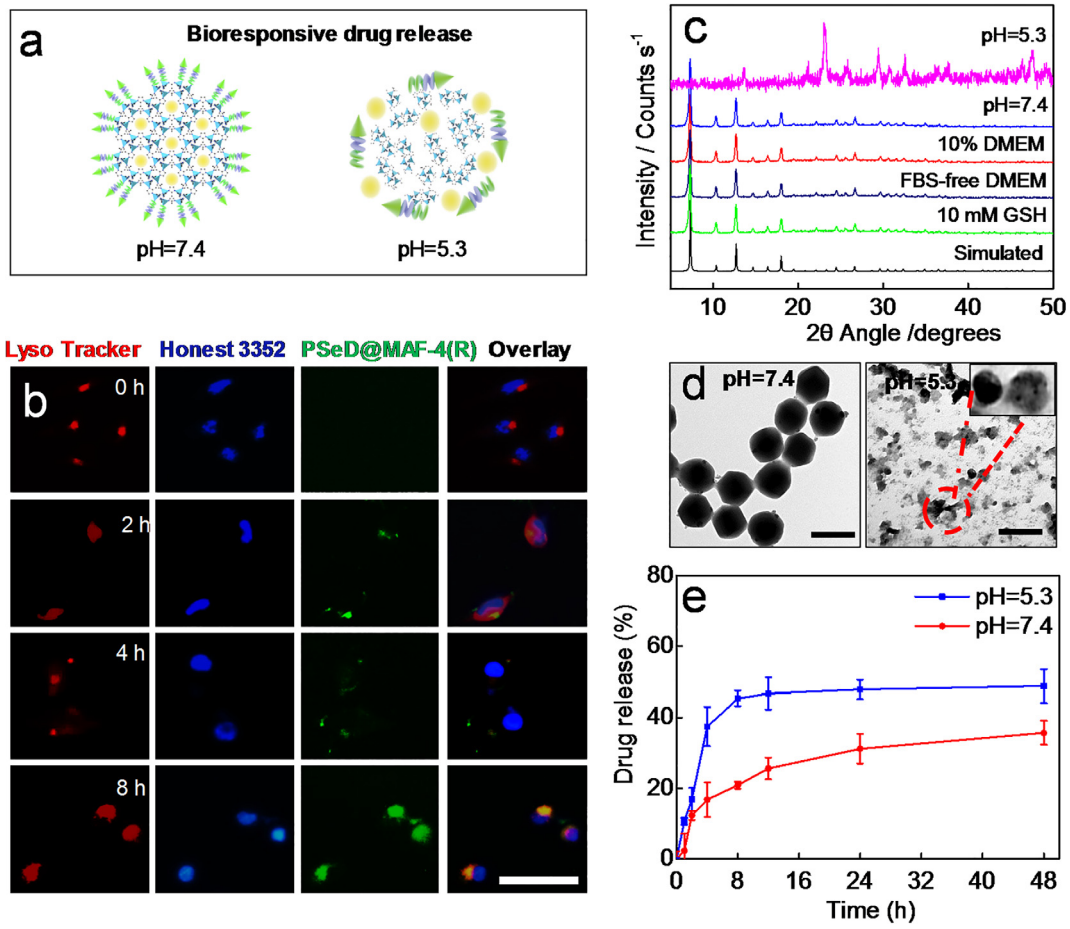

Fig. 2. a) Simulated bioresponsive drug release of PSeD@MAF-4(R). b) Intracellular localization of PSeD@MAF-4(R) in living cells. c) PXRD of MAF-4 simulated, and PSeD@MAF-4(R) under various tested conditions. d) TEM images of PSeD@MAF-4(R) in different buffers. e) *In vitro* drug release of PSeD from PSeD@MAF-4(R) in different pH. Each value represents means ± SD (n = 3).

higher cellular uptake and rapid drug accumulation. [31] Taken together, MAF-4 was a pH-sensitive nanocarrier system with responsibility to cancer microenvironment.

PSeD@MAF-4(R) is proposed to recognize $\alpha_v\beta_3$ integrin receptor by the cRGD targeting peptide to distinguish tumor cells from normal cells, and then accumulated to the tumor sites during blood circulation (Fig. 3a). Therefore, western blot experiment was done to proof the overexpression of $\alpha_v\beta_3$ integrin in MCF-7 cells (Fig. S6a), and the targeting property was further confirmed by cRGD blocking assay and cell survival study. As shown in Fig. S6a, after preincubation with cRGD, the amount of PSeD@MAF-4(R) absorbed by MCF-7 cells decreased significantly, which may be due to the interaction of cRGD with $\alpha_v\beta_3$ integrin receptor and thus inhibited the recognition by PSeD@MAF-4(R). Consistently, the cell viability increased with increasing of cRGD concentration (Fig. S6b).

In order to evaluate the anticancer activity of PSeD@MAF-4(R), *in vitro* experiments were carried out using MTT assay. As shown in Fig. 3b, beside MCF-7 cells, PSeD@MAF-4(R) shown broad anticancer activities against A549 nonsmall-cell lung cancer cells, Siha cervical cancer cells, MB-231 triple-negative breast cancer cells, while shown low toxicity to normal cells (HUVEC, HL-7702 and L02 cells). The safety index was found reaching 15.1, much higher than those of commercial anticancer drugs. Moreover, the anticancer activity of PSeD@MAF-4(R) was also much higher than those of free PSeD (Fig. 3b), while the naked MAF-4 showed negligible toxicity (Fig. S6c). As comparison, we also determined the cellular uptake of the naked MAF-4 and PSeD@MAF-4(R) (40 μM) in different cell lines for different time intervals by ICP-MS analysis of Se content. As shown in Fig. 3c, the time of maximum PSeD uptake was 4 h, while great difference was also found in Se content in cancer and normal cells. These results confirmed the high cancer selectivity of PSeD@MAF-4(R).

In order to get more insight into the action mechanisms, flow cytometry was used to analyze the cell cycle distribution. From Figs. 3d and S7a we can see, free PSeD slightly induced cell apoptosis and G2/M arrest, while PSeD@MAF-4 and PSeD@MAF-4(R) significantly caused cumulative sub-G1 (78.5% and 90.5%, respectively). This suggested that induction of apoptosis was the major action mode for the targeting PSeD@MAF-4(R). Overproduction of reactive oxygen species (ROS) is very important to understand the cell apoptosis pathway. Intracellular ROS could cause protein, DNA damage, and induce apoptosis. Therefore, we have detected the ROS level by DHE fluorescence probe. As shown in Fig. 3e, intracellular ROS produced by PSeD@MAF-4(R) reached 200% at 70 min, then decreased to 165% (135 min), while that produced by PSeD found at about 138%. This indicated that PSeD@MAF-4(R) can significantly enhance the intracellular ROS production. Consistently, as shown in Figs. 3f and S7b, both MAF-4 nanocarrier and naked PSeD produced less amount of ROS, but PSeD@MAF-4(R) produced much higher ROS fluorescence. As we known, ROS are strong oxidants. It will oxidize reducing agent such as glutathione (GSH), so we further do quantitative analysis on the effects of GSH. As shown in Fig. S8a, when GSH was added to the PSeD@MAF-4(R) system, the fluorescence caused by the generated ROS was significantly decreased from 149% to 110%. As excessive ROS can cause apoptotic cell death, we further determined the effects of GSH on PSeD@MAF-4(R)-induced cytotoxicity. As shown in Fig. S8b, addition of GSH effectively increased the cell viability from 19.1% to 73.5%. All these results suggested that

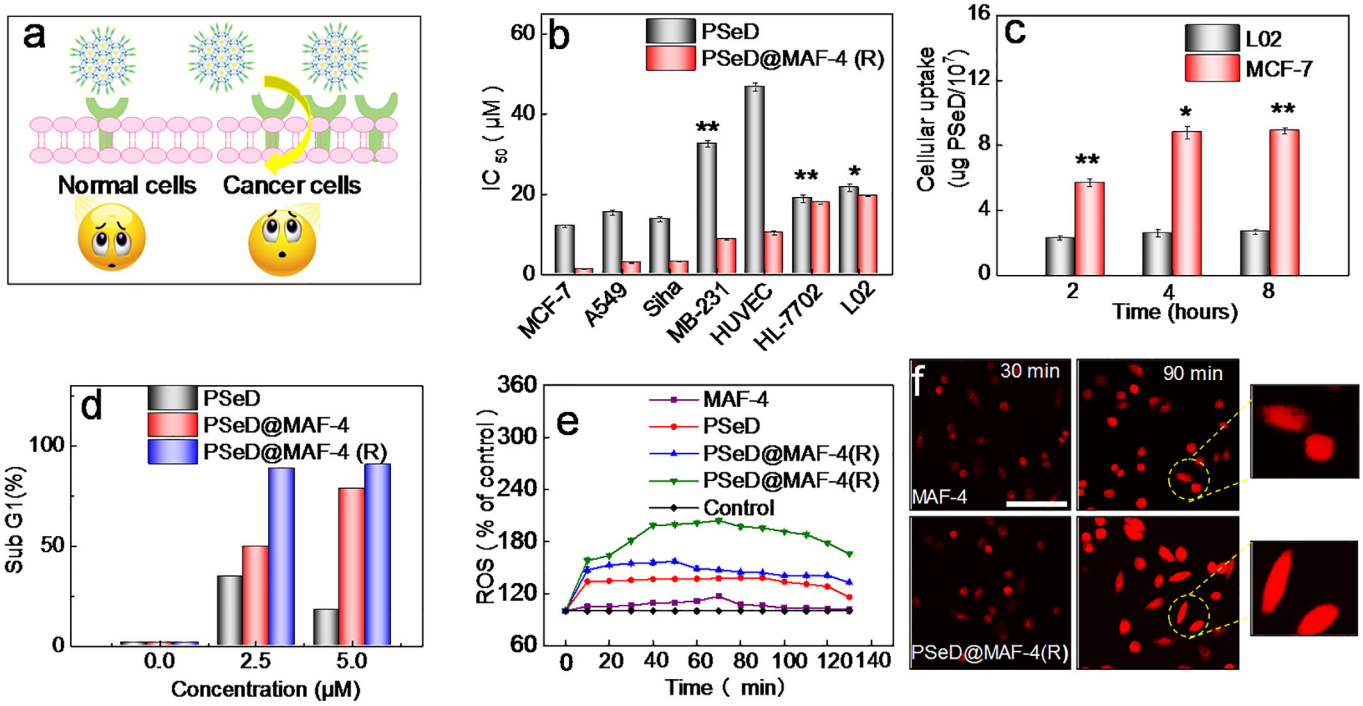

Fig. 3. a) Selective induction of cancer cells apoptosis by PSeD@MAF-4(R). b) IC_{50} of PSeD and PSeD@MAF-4(R) on various human cancer and normal cells. c) Selective uptake of PSeD@MAF-4(R) (40 μM) by MCF-7 and L02. d) Flow cytometric analysis of MCF-7 cell apoptosis. e) ROS generation induced by MAF-4 (5.0 μM), PSeD (5.0 μM), PSeD@MAF-4(R) (25, 50 μM) in MCF-7 cells. f) Fluorescent ROS in MCF-7 after incubated with MAF-4 (50 μM), PSeD (50 μM), PSeD@MAF-4(R) (50 μM) different periods of time. scale bar = 100 μm. Each value represents means ± SD (n = 3).

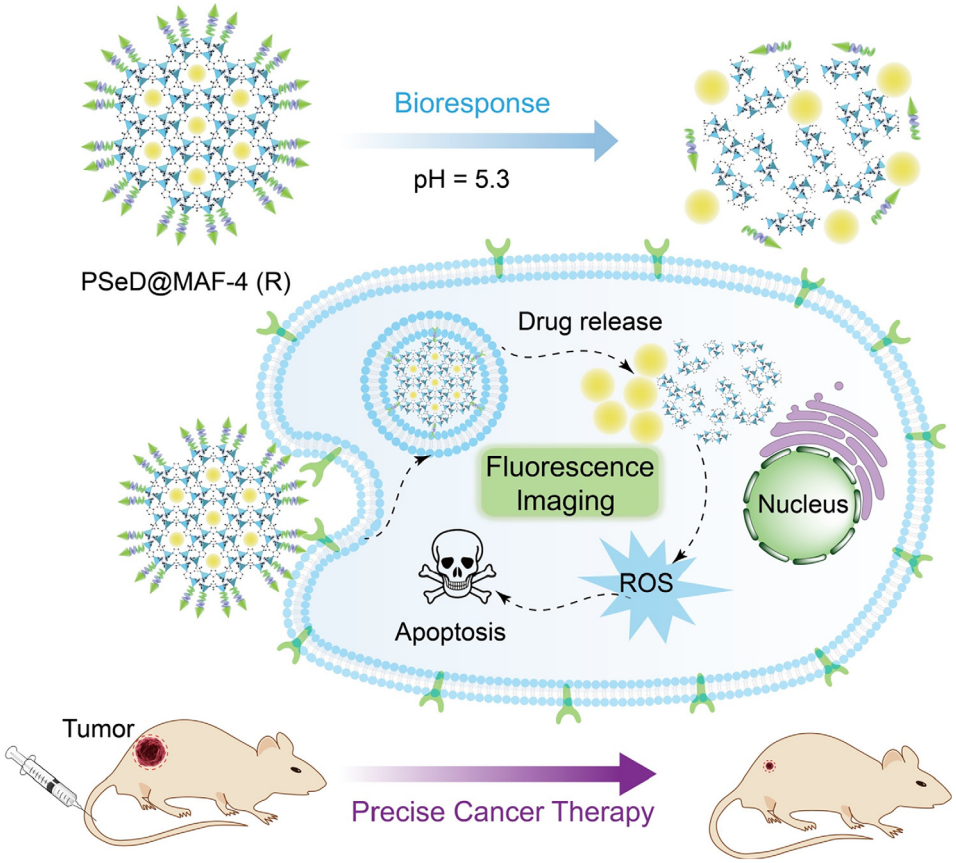

Scheme 1. The demonstration of PSeD@NMAF-4(R) nanosystem bioresponsive release drug PSeD to precise treatment of breast cancer.

PSeD@MAF-4(R) caused overproduction of ROS to induce cancer cell apoptosis.

Encouraged by the remarkable efficacy of PSeD@MAF-4(R) *in vitro* and to ascertain the biocompatibility of PSeD@MAF-4(R), we investigated the therapeutic effect of this systems in nude mice with MCF-7 xenograft (Figs. S9–S11). The detailed results were discussed in Supporting information and the whole results indicate the potent antitumor potential of PSeD@MAF-4(R) without obvious side effects.

In summary (Scheme 1), herein we reported a novel strategy of a cancer-targeted MAF nanosystem, PSeD@MAF-4(R), which displayed pH-dependent decomposition behavior and high drug loading capability. Anticancer drugs could be encapsulated into this nanosystem with a high loading rate at 16.1%, and grafted with PEI-PEG-derived cRGD peptide to enhance biocompatibility [32] and cancer selectivity. Furthermore, MAF-4 nanosystem possessed pH-responsive property, leading to drug release in cancer microenvironment. The PSeD@MAF-4(R) specifically accumulates in tumors *in vivo*, and thus demonstrates high antitumor efficacy, but non-toxic to normal tissues, possibly due to the non-toxic composition of the ligand and zinc that constitute MAF-4. Taken together, this study provided an innovative strategy for precise cancer therapy using nanoscale MAF materials and inspired further researchers in this fast-developing field.

Acknowledgements

This work was supported by Natural Science Foundation of China (21877049 and 21701054), National Program for Support of Top-notch Young Professionals (W02070191), YangFan Innovative & Entepreneurial Research Team Project (201312H05), Fundamental Research Funds for the Central Universities.

Competing interests

The authors declare that they have no competing interests.

Appendix A. Supplementary data

Supplementary data to this article can be found online at https://doi.org/10.1016/j.cej.2019.04.016.

References

[1] J. Ferlay, E. Steliarove-Foucher, J. Lortet-Tieulent, S. Rosso, J.W.W. Coebergh, H. Comber, D. Forman, F. Bray, Cancer incidence and mortality patterns in Europe: estimates for 40 countries in 2012, Eur. J. Cancer 49 (2013) 1374–1403.
[2] Y. Hashimoto, S. Tatsumi, R. Takeda, A. Naka, N. Ogane, Y. Kameda, K. Kawachi, S. Shimizu, M. Sakai, S. Kamoshida, Expression of organic anion-transporting polypeptide 1A2 and organic cation transporter 6 as a predictor of pathologic response to neoadjuvant chemotherapy in triple negative breast cancer, Breast Cancer Res. Treat. 145 (2014) 101–111.
[3] S. Liu, Radiolabeled cyclic RGD peptides as integrin αvβ3-targeted radiotracers: maximizing binding affinity via bivalency, Bioconjugate Chem. 20 (2009) 2199–2213.
[4] M. Zhou, S. Ji, Z. Wu, Y. Li, W. Zheng, H. Zhou, T. Chen, Synthesis of selenazolopyridine derivatives with capability to induce apoptosis in human breast carcinoma MCF-7 cells through scavenge of intracellular ROS, Eur. J. Med. Chem. 96 (2015) 92–97.
[5] Y. Wang, W. Li, Y. Yang, Q. Zeng, K.H. Wong, X. Li, T. Chen, An integrin-targeting nanosystem as a carrier of the selenadiazole derivative to induce ROS-mediated apoptosis in bladder cancer cells, from rational design to action mechanisms, J. Mater. Chem. B 3 (2015) 9374–9382.
[6] Y. Liang, Y. Zhou, S. Deng, T. Chen, Microwave-assisted syntheses of benzimidazole-containing selenadiazole derivatives that induce cell-cycle arrest and apoptosis in human breast cancer cells by activation of the ROS/AKT pathway, ChemMedChem 11 (2016) 2339–2346.
[7] M. Faria, M. Björnmalm, K.J. Thurecht, S.J. Kent, R.G. Parton, M. Kavallaris, A.P.R. Johnston, J.J. Gooding, S.R. Corrie, B.J. Boyd, P. Thordarson, A.K. Whittaker, M.M. Stevens, C.A. Prestidge, C.J.H. Porter, W.J. Parak, T.P. Davis, E.J. Crampin, F. Caruso, Minimum information reporting in bio-nano experimental literature, Nat. Nanotechnol. 13 (2018) 777–785.
[8] P. Hirschle, T. Preiß, F. Auras, A. Pick, J. Völkner, D. Valdepérez, G. Witte, W.J. Parak, J.O. Rädler, S. Wuttke, Exploration of MOF nanoparticle sizes using various physical characterization methods – is what you measure what you get? CrysEngComm 18 (2016) 4359–4368.
[9] T. Simon-Yarza, A. Mielcarek, P. Couvreur, C. Serre, Nanoparticles of metal-organic frameworks: on the road to in vivo efficacy in biomedicine, Adv. Mater. 30 (2018) 1707365.
[10] S. Wang, C.M. McGuirk, A. d'Aquino, J.A. Mason, C.A. Mirkin, Metal-organic framework nanoparticles, Adv. Mater. 30 (2018) 1800202.
[11] R. Freund, U. Lächelt, T. Gruber, B. Rühle, S. Wuttke, Multifunctional efficiency: extending the concept of atom economy to functional nanomaterials, ACS Nano 12 (2018) 2094–2105.
[12] S. Wuttke, M. Lismont, A. Escudero, B. Rungtaweevoranit, W.J. Parak, Positioning metal-organic framework nanoparticles within the context of drug delivery – a comparison with mesoporous silica nanoparticles and dendrimers, Biomaterials 123 (2017) 172–183.
[13] S. Wuttke, A. Zimpel, T. Bein, S. Braig, K. Stoiber, A. Vollmar, D. Müller, K. Haastert-Talini, J. Schaeske, M. Stiesch, G. Zahn, A. Mohmeyer, P. Behrens, O. Eickelberg, D.A. Bölükbas, S. Meiners, Validating metal-organic framework nanoparticles for their nanosafety in diverse biomedical applications, Adv. Healthcare Mater. 6 (2016) 1600818.
[14] A.X. Zhu, R.B. Lin, X.L. Qi, Y. Liu, Y.Y. Lin, J.P. Zhang, X.M. Chen, Zeolitic metal azolate frameworks (MAFs) from $ZnO/Zn(OH)_2$ and monoalkyl-substituted imidazoles and 1,2,4-triazoles: Efficient syntheses and properties, Microporous Mesoporous Mater. 157 (2012) 42–49.
[15] T. Tian, Z. Zeng, D. Vulpe, M.E. Casco, G. Divitini, P.A. Midgley, J. Silvestre-Albero, J.C. Tan, P.Z. Moghadam, D. Fairen-Jimenez, A sol–gel monolithic metal–organic framework with enhanced methane uptake, Nat. Mater. 17 (2018) 174–179.
[16] H. Li, M. Eddaoudi, M. O'Keeffe, O.M. Yaghi, Design and synthesis of an exceptionally stable and highly porous metal-organic framework, Nature 402 (1999) 276–279.
[17] J. Lee, O.K. Farha, J. Roberts, K.A. Scheidt, S.T. Nguyen, J.T. Hupp, Metal–organic framework materials as catalysts, Chem. Soc. Rev. 38 (2009) 1450–1459.
[18] J. Drocca, D. Liu, W.B. Lin, Nanoscale metal-organic frameworks for biomedical imaging and drug delivery, Acc. Chem. Res. 44 (2011) 957–968.
[19] W. Cai, C.C. Chu, G. Liu, Y.X. Wang, Metal-organic framework-based nanomedicine platforms for drug delivery and molecular imaging, Small 11 (2015) 4806–4822.
[20] L. Wang, M. Zheng, Z. Xie, Nanoscale metal–organic frameworks for drug delivery: a conventional platform with new promise, J. Mater. Chem. B 6 (2018) 707–717.
[21] P. Horcajada, T. Chalati, C. Serre, B. Gillet, C. Sebrie, T. Baati, J.F. Eubank, D. Heurtaux, P. Clayette, C. Kreuz, J.S. Chang, Y.K. Hwang, V. Marsaud, P.N. Bories, L. Cynober, S. Gil, G. Ferey, P. Couvreur, R. Gref, Porous metal–organic-framework nanoscale carriers as a potential platform for drug delivery and imaging, Nat. Mater. 9 (2010) 172–178.
[22] S.H. Jhung, J.H. Lee, J.W. Yoon, C. Serre, G. Ferey, J.S. Chang, Microwave synthesis of chromium terephthalate MIL-101 and its benzene sorption ability, Adv. Mater. 19 (2007) 121–124.
[23] C. He, K. Lu, D. Liu, W. Lin, Nanoscale metal-organic frameworks for the co-delivery of cisplatin and pooled siRNAs to enhance therapeutic efficacy in drug-resistant ovarian cancer cells, J. Am. Chem. Soc. 136 (2014) 5181–5184.
[24] D. Zhao, J.L. Shui, L.R. Grabstanowicz, C. Chen, S.M. Commet, T. Xu, J. Lu, D.J. Liu, Highly efficient non-precious metal electrocatalysts prepared from one-pot synthesized zeolitic imidazolate frameworks, Adv. Mater. 26 (2014) 1093–1097.
[25] Z.Y. Jiang, H.L. Liu, S.A. Ahmed, S. Hanif, S.B. Ren, J.J. Xu, H.Y. Chen, X.H. Xia, K. Wang, Insight into ion transfer through the sub-nanometer channels in zeolitic imidazolate frameworks, Angew. Chem. Int. Ed. 56 (2017) 4767–4771.
[26] W.H. Chen, X. Yu, W.C. Liao, Y.S. Sohn, A. Cecconello, A. Kozell, R. Nechushtai, I. Willner, ATP-responsive aptamer-based metal-organic framework nanoparticles (NMOFs) for the controlled release of loads and drugs, Adv. Funct. Mater. 27 (2017) 1702102.
[27] C. He, C. Poon, C. Chan, S.D. Yamada, W. Lin, Nanoscale coordination polymers codeliver chemotherapeutics and siRNAs to eradicate tumors of cisplatin-resistant ovarian cancer, J. Am. Chem. Soc. 138 (2016) 6010–6019.
[28] J. Park, Q. Jiang, D.W. Feng, L.Q. Mao, H.C. Zhou, Size-controlled synthesis of porphyrinic metal-organic framework and functionalization for targeted photodynamic therapy, J. Am. Chem. Soc. 138 (2016) 3518–3525.
[29] C.B. He, D.M. Liu, W.B. Lin, Nanomedicine applications of hybrid nanomaterials built from metal-ligand coordination bonds: nanoscale metal-organic frameworks and nanoscale coordination polymers, Chem. Rev. 115 (2015) 11079–11108.
[30] X.C. Ma, J.L. Jia, R. Cao, X.B. Wang, H. Fei, Histidine–iridium(III) coordination-based peptide luminogenic cyclization and cyclo-RGD peptides for cancer-cell targeting, J. Am. Chem. Soc. 136 (2014) 17734–17737.
[31] X.Z. Yang, X.J. Du, Y. Liu, Y.H. Zhu, Y.Z. Liu, Y.P. Li, J. Wang, Rational design of polyion complex nanoparticles to overcome cisplatin resistance in cancer therapy, Adv. Mater. 26 (2014) 931–936.
[32] C. Zhang, K.L. Zhao, W.B. Bu, D.L. Ni, Y.Y. Liu, J.W. Feng, J.L. Shi, Marriage of scintillator and semiconductor for synchronous radiotherapy and deep photodynamic therapy with diminished oxygen dependence, Angew. Chem. Int. Ed. 54 (2015) 1770–1774.